Earth Observation Image Librarian

FEATURE EXTRACTION ALGORITHMS TECHNICAL NOTE

Prepared By	Jagmal Singh	2014-09-24 Date
	Daniela Espinoza-Molina	2014-10-02 Date
	Shiyong Cui	Date
Reviewed By		Date
Released By		Date

Deutsches Zentrum für Luft- und Raumfahrt e.V.
in der Helmholtz-Gemeinschaft

DOCUMENT CHANGE RECORD

Issue	Date	Where	Change
0.5	2014-07-14	all	Draft version for Progress Meeting #7
1.0	2014-10-03		Update and release for CDR

TABLE OF CONTENTS

LIST OF FIGURES

1. Introduction

1.1 Purpose & Scope

This technical note (TN) provides theoretical details of the selected feature extraction algorithms for detected (DET) synthetic aperture radar (SAR) images. Implementation of feature extraction algorithms is a part of Data Model Generation (DMG) modules of the EOLib's service components [AD01]. DMG module focuses on the content and context analysis of the different Earth observation (EO) sources. Different feature extraction methods are considered in the case of image content. The features extracted from the images are complemented with image metadata (extracted from the XML file of the product) and geometrical and topological data (e.g., GIS data).

The feature extraction methods are classified according to the input data. Following categories are identified in [AD02]:

a) Feature extraction for optical images
b) Feature extraction for synthetic aperture radar (SAR) images
c) Feature extraction for Polarimetric SAR (PolSAR) data
d) Feature extraction for Image Time Series (ITS)
e) Feature extraction for geometrical and topological analysis

This TN describes the theoretical overview of the feature extraction algorithms, in the current issue only for (b), i.e. SAR images. The feature extraction algorithms will read the original L1b EO products (e.g., for detected (DET) and geocoded TerraSAR-X products are unsigned 16 bits). The algorithms are applied to full scene and the analyzing window (as a parameter) of the algorithms is the size of the patch. Three feature extraction algorithms are presented in this TN. First two are based on the Gabor filter banks, and third one is adaptation of the Weber local descriptor (WLD) for SAR images.

This TN will be updated in a future release with the description for multispectral feature extraction algorithm that will be used for EOLib.

1.2 Applicable Document/s

The following project documents contain provisions which, through reference in this text, become applicable to the extent specified in this document.

[AD01]	EOLib Architecture Concept	EOLIB-TN-DLR-3100 Issue 1.1, 2013-04-04
[AD02]	EOLib Algorithm Specification	EOLIB-TN-DLR-3300 Issue 1.5, 2013-12-03
[AD03]	EOLib Image Information Mining Algorithm Design	EOLIB-TN-DLR-4401 Issue 0.1, 2014-xx-xx

1.3 Document Overview

This document is structured as follows:

Chapter 1	This introduction
Chapter 2	Feature Extraction Algorithms
Chapter 3	Implementation
Appendix A	Abbreviations
Appendix B	References

2. Feature Extraction Algorithms

2.1 Introduction

Feature extraction algorithms can be divided into two classes (Chen, et al., 2010): one is a dense descriptor which extracts local features pixel by pixel over the input image (Randen & Husoy, 1999), the other is a sparse descriptor which first detects the interest points in a given image and then samples a local patch and describes its invariant features (Mikolajczyk & Schmid, 2005). We have identified the Gabor filter banks based dense descriptor and adapted a Weber local descriptor (A-WLD) based sparse descriptor as appropriate feature extraction methods for detected SAR images.

2.2 Gabor filter banks

Gabor expansion was introduced by a Hungarian-born British physicist, Dennis Gabor in 1946, particularly suitable for analysis of signals with sharp changes but which stay for a small duration of time. It suggests expanding a signal into a set of functions that are concentrated in both time and frequency (Gabor, 1946). This set of functions, also called the Gabor coefficients, plays the main role in analysis of signal's local properties. Gabor expansion can be written mathematically as follows (Qian & Chen, 1993):

$$s(t) = \sum_{m=-\infty}^{\infty} \sum_{n=-\infty}^{\infty} G_{m,n} h_{m,n}(t), \text{ with } h_{m,n}(t) = h(t - mT) e^{jn\omega t}.$$

Where, $G_{m,n}$ are called the Gabor coefficients. The set of elementary functions $h_{m,n}(t)$ consists of a time-frequency shifted function $h(t)$. In practice, to describe the texture of an image $i(x, y)$, a filter structure is employed where image is filtered using the band pass filters, also called Gabor elementary functions (GEF) $h(x, y)$ to extract a specific frequency band from an image. Usually a convolution operation $(*)$ of GEF's,$h(x, y)$, with the original image, $i(x, y)$, is employed to obtain a Gabor filtered image, m(x, y), as follows:

$$m(x, y) = |i(x, y) * h(x, y)|.$$

Description of the Gabor elementary functions

Gabor coefficients or GEF's are not unique and can be described in many different ways. GEF's are sometimes also referred as Gabor wavelets, which are nothing but the Gaussian modulated by a complex sinusoid as follows (Super & Bovik, 1991), (Bovik, et al., 1990):

$$h(x, y) = g(x', y') e^{j2\pi(Ux + Vy)}.$$

Here, $(x', y') = (x \cos \emptyset + j \sin \emptyset, -x \sin \emptyset + j \cos \emptyset)$ are the rotated rectilinear coordinates in spatial domain, and (U, V) are the particular 2-D frequencies in the complex-sinusoid. The 2-D Gaussian function $g(x, y)$ with its corresponding Fourier transform $G(u, v)$ is given as (Dunn, et al., 1994):

$$g(x, y) = \frac{1}{2\pi\sigma_x\sigma_y} \exp\left[-\frac{1}{2}\left(\frac{x^2}{\sigma_u^2} + \frac{y^2}{\sigma_v^2}\right)\right],$$
$$G(u, v) = \exp\left\{-2\pi^2\left[(\sigma_x[u - U]')^2 + \left(\sigma_y[v - V]'\right)^2\right]\right\}.$$

Here, $([u - U]', [v - V]') = [(u - U)\cos\theta + (v - V)\sin\theta, -(u - U)\sin\theta + (v - V)\cos\theta]$, are the shifted and rotated rectilinear coordinates in the frequency-domain, with $\sigma_u = 1/2\pi\sigma_x, \sigma_v = 1/2\pi\sigma_y$ characterizing the spatial extent and bandwidth of $h(x, y)$. Filter parameters (σ_u and σ_v) can be computed in several ways. The Gabor wavelets are non-orthogonal in nature unless they are poorly concentrated in time or in frequency domain. While keeping a good time and frequency domain concentration, nonorthogonality is

allowed at the cost of redundant information in the filtered image. In order to reduce this redundancy, following formulation to compute σ_u and σ_v has been proposed in (Manjunath & Ma, 1996):

$$\sigma_u = \frac{\left((U_h/U_l)^{\frac{1}{S-1}} - 1\right) U_h}{\left((U_h/U_l)^{\frac{1}{S-1}} + 1\right)\sqrt{2\log 2}},$$

$$\sigma_v = \tan\left(\frac{\pi}{2O}\right)\left[U_h - 2\log\left(\frac{2\sigma_u^2}{U_h}\right)\right]\left[2\log 2 - \frac{(2\log 2)^2\sigma_u^2}{U_h^2}\right]^{-\frac{1}{2}}.$$

Here, U_h and U_l are the upper and lower center frequencies of interest in the Gabor kernel, S is the number of stages and O is the number of orientations used in the multi-scale/ multi-resolution Gabor decomposition. The choice of Gabor coefficients is not restrictive but the foundations for wide usage of Gabor filter banks for texture description were mainly laid in (Manjunath & Ma, 1996) with the proposal of a homogeneous texture (HT) descriptor, and later advocated in diverse fields studies (Kandaswamy, et al., 2005), (Riaz, et al., 2012). We also followed the same formulation, with U_h= 0.45, U_l= 0.05. In the Figure 2-1, we illustrate the examples of real and imaginary parts of the Gabor kernel at stage S = 1, and six different orientations O = 1, 2, · · ·, 6. The SAR image under consideration, is convolved with this complex-valued Gabor filter bank to obtain a Gabor filtered image.

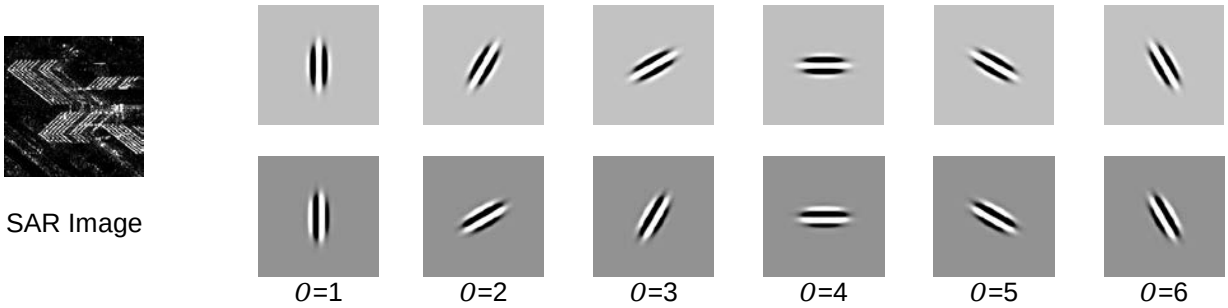

Figure 2-1: SAR image is convolved with the Gabor filter banks to get a Gabor filter image. Shown are (top) the real part and (bottom) the imaginary part of the Gabor kernel for a particular stage **S** = 1, and six different orientations **O** = 1,2,⋯,6.

Convolution of SAR image with complex-valued Gabor coefficients will provide us a complex-valued Gabor filtered output. The amplitude of this filtered output is used to generate a feature descriptor.

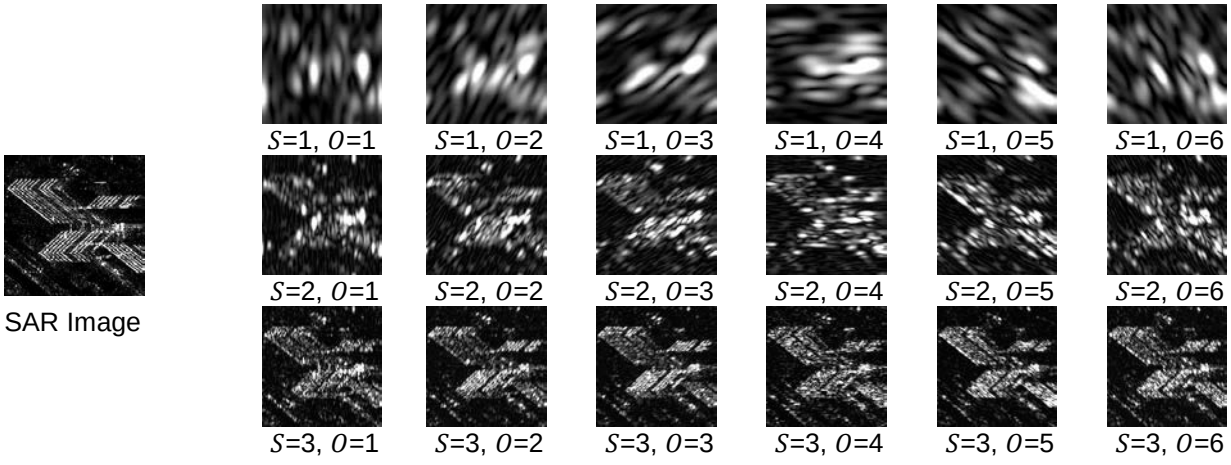

Figure 2-2: SAR image is convolved with the Gabor filter banks to get a Gabor filter image. The amplitudes of the Gabor filtered images using 3 stages and 6 orientations are shown.

2.2.1 *Feature descriptor based on moments of Gabor filtered images*

Even for the Gabor filters applied to DET SAR images, we will obtain complex-valued filtered images. As it has been commented in (Julesz, 1981), that only linear mechanisms are not sufficient to explain how human visual system perceives the texture, to further incorporate non-linearity in the Gabor based approach, one idea is to work on the amplitude of the complex-valued sub-images. In (Bovik, et al., 1990), as well as in (Manjunath & Ma, 1996), it has been studied extensively that amplitude of the complex-valued sub-images can be used to characterize the texture of images. Now the obvious choices for a feature descriptor over the amplitude of the filtered images are the simple statistical measure, i.e. mean μ and variance σ^2. Thus, we also compute the moments of the amplitude of the complex-valued Gabor filtered output at different scales and orientations, which later constitutes the feature descriptor.

The invariance properties of Gabor filters along with the restrictions to the use of Gabor filters for feature extraction have been demonstrated in (Kamarainen, et al., 2006). Even though a lot of study have been carried out since the Gabor expansion with the proposal of some recent feature descriptor based on Gabor filters such as auto-correlation Gabor features (Riaz, et al., 2012) etc., the use of moments of the Gabor filtered images are still widely accepted tool for texture synthesis in multimedia as well as remote sensing images. The homogeneous texture descriptor under the visual texture descriptor in the moving picture experts group (MPEG)- 7 standard (Sikora, 2001) also rely on this feature descriptor, thus can be considered as a benchmarking tool for comparing alternative methodologies.

In EOLib project deliverables, we have used 4 stages, and 6 orientations, with U_h= 0.45, U_l= 0.05 in Gabor filter bank formation. For 4 stages, and 6 orientations, we obtain a feature descriptor of length 48:

$$\bar{f}_{Gabor_{\mu,\sigma^2}} = \begin{matrix}\{\mu_{1,1}, {\sigma^2}_{1,1}, \mu_{1,2}, {\sigma^2}_{1,2}, \mu_{1,3}, {\sigma^2}_{1,3}, \mu_{1,4}, {\sigma^2}_{1,4}, \mu_{1,5}, {\sigma^2}_{1,5}, \mu_{1,6}, {\sigma^2}_{1,6}, \\ \dots, \mu_{4,1}, {\sigma^2}_{4,1}, \mu_{4,2}, {\sigma^2}_{4,2}, \mu_{4,3}, {\sigma^2}_{4,3}, \mu_{4,4}, {\sigma^2}_{4,4}, \mu_{4,5}, {\sigma^2}_{4,5}, \mu_{4,6}, {\sigma^2}_{4,6}\}.\end{matrix}$$

With, $\mu_{S,O}$, ${\sigma^2}_{S,O}$ are the first two moments (mean and variance, respectively) of Gabor filtered image at stage-S, orientation-O.

2.2.2 *Feature descriptor based on logarithmic-cumulants of Gabor filtered images*

Based on the method of log-cumulants (MoLC) (Nicolas, 2002), we proposed in (Singh & Datcu, 2013) to enhance the accuracy of patch indexing using the log- cumulants of Gabor filtered images, instead of their moments. Let $Gabor_{S,O}(\cdot)$ be the Gabor filtered image at a stage S, and orientation O. For an image $i(x,y)$ of size $M \times N$, the first three logarithmic-cumulants $(\tilde{\kappa}1_{S,O}, \tilde{\kappa}2_{S,O} \text{ and } \tilde{\kappa}3_{S,O})$ for the amplitude-envelope of the Gabor filtered image at this stage and orientation are estimated as follows:

$$\tilde{\kappa}1_{S,O} = \frac{1}{M \times N} \sum_{u=1}^{M} \sum_{v=1}^{N} \ln\left(\left|Gabor_{S,O}\left(i(x,y)\right)\right|\right),$$

$$\tilde{\kappa}2_{S,O} = \frac{1}{(M \times N - 1)} \sum_{u=1}^{M} \sum_{v=1}^{N} \ln\left(\left|Gabor_{S,O}\left(i(x,y)\right)\right| - \tilde{\kappa}1_{S,O}\right)^2,$$

$$\tilde{\kappa}3_{S,O} = \frac{M \times N}{(M \times N - 1)(M \times N - 2)} \sum_{u=1}^{M} \sum_{v=1}^{N} \ln\left(\left|Gabor_{S,O}\left(i(x,y)\right)\right| - \tilde{\kappa}1_{S,O}\right)^3,$$

In EOLib project deliverables, we have used 4 stages, and 6 orientations, with U_h= 0.45, U_l= 0.05 in Gabor filter bank formation. For 4 stages, and 6 orientations, we obtain a feature descriptor of length 48:

$$\bar{f}_{Gabor_{\tilde{\kappa}1,\tilde{\kappa}2}} = \begin{matrix}\{\tilde{\kappa}1_{1,1}, \tilde{\kappa}2_{1,1}, \tilde{\kappa}1_{1,2}, \tilde{\kappa}2_{1,2}, \tilde{\kappa}1_{1,3}, \tilde{\kappa}2_{1,3}, \tilde{\kappa}1_{1,4}, \tilde{\kappa}2_{1,4}, \tilde{\kappa}1_{1,5}, \tilde{\kappa}2_{1,5}, \tilde{\kappa}1_{1,6}, \tilde{\kappa}2_{1,6}, \\ \dots, \tilde{\kappa}1_{4,1}, \tilde{\kappa}2_{4,1}, \tilde{\kappa}1_{4,2}, \tilde{\kappa}2_{4,2}, \tilde{\kappa}1_{4,3}, \tilde{\kappa}2_{4,3}, \tilde{\kappa}1_{4,4}, \tilde{\kappa}2_{4,4}, \tilde{\kappa}1_{4,5}, \tilde{\kappa}2_{4,5}, \tilde{\kappa}1_{4,6}, \tilde{\kappa}2_{4,6}\}.\end{matrix}$$

With, $\tilde{\kappa}1_{S,O}$, $\tilde{\kappa}2_{S,O}$ are the first two log-cumulants estimates of Gabor filtered image at stage-S, orientation-O.

2.3 Adapted Weber Local Descriptor

WLD was proposed in (Chen, et al., 2010) for optical image retrieval by the inspiration of Weber's law, which states that the change of a stimulus that will be just noticeable is a constant ratio of the original stimulus. If the change is smaller than this constant ratio, it cannot be recognized. Based on this idea, WLD is proposed for texture characterization, which is composed of two components: differential excitation ξ and orientation θ. The differential excitation is defined as:

$$\xi(x_c) = \arctan\left[\sum_{i=0}^{n-1}\left(\frac{x_i - x_c}{x_c}\right)\right].$$

Here, n is the number of neighboring pixels, which are 8 in the case of Figure 2-3(a). The orientation is given as the gradient orientation, defined by:

$$\theta(x_c) = \arctan\left(\frac{x_7 - x_3}{x_5 - x_1}\right).$$

Based on the two terms, a joint histogram can be constructed, followed by converting it to a one dimensional histogram, which is the WLD. The advantage of this feature is that it considers not only the local contrast but also the structure information represented by gradient histogram. Although Weber's law is a theory from visual perception and there is no visual aspect for SAR images, the principle for feature extraction is still applicable to SAR images. Nevertheless, in the case of SAR images, multiplicative speckle noise decreases dramatically its discriminative ability for image indexing. To combat against speckle, we proposed a solution (Cui, et al., 2013) to replace the gradient in WLD by the ratio of mean differences (RMD). RMD is computation is based on the ratio detector (Touzi, et al., 1988). The ratio detector is defined as the ratio of the means of two neighborhoods on the opposite sides of the point. To detect all possible edges, the ratio detector should be applied in all possible directions. The edge response for a pixel is the maximum of all the edge responses in all directions. For the sake of computation, a local window centered at a pixel is split into two contiguous neighborhoods. Four principal directions $i = 0, \dots, 3$, i.e. $0^{\circ}, 45^{\circ}, 90^{\circ}, 135^{\circ}$ are assumed in Figure 2-3 and the ratios of local means (μ_1^i, μ_2^i) of the two neighborhoods are computed.

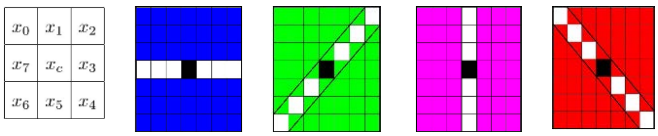

Figure 2-3: Eight neighborhoods and four directions (0°,45°,90°,135°) used for the definition of SAR image ratio detector.

The edge responses of the four principal directions are defined as:

$$r^i = 1 - \min\left(\mu_1^i/\mu_2^i, \mu_2^i/\mu_1^i\right), i = 0, \dots, 3.$$

The final edge response for a pixel is give as $R = \max(r^i), i = 0, \cdots, 3$, which is referred as mean ratio. Based on the ratio detector, the RMD is defined as:

$$R_{SAR} = D_v/D_h = (\mu_1^1 - \mu_2^1)/(\mu_1^3 - \mu_2^3).$$

Where, $D_v = \mu_1^1 - \mu_2^1$ and $D_h = \mu_1^3 - \mu_2^3$ are the differences of the local means of the two neighborhoods corresponding to both vertical and horizontal directions, the two blue and magenta regions shown in the Figure 2-3(b) and (d). The RMD can be considered as an adaptation of the gradient for SAR images, leading to the following adapted orientation component and differential excitation:

$$\theta(x_c) = \arctan2(R_{SAR}) = \arctan2(D_v/D_h), \qquad \xi(x_c) = \arctan\left[\sum_{i=0}^{3}\sum_{j=0}^{2}\left(\frac{\mu_j^i - x_c}{x_c}\right)\right].$$

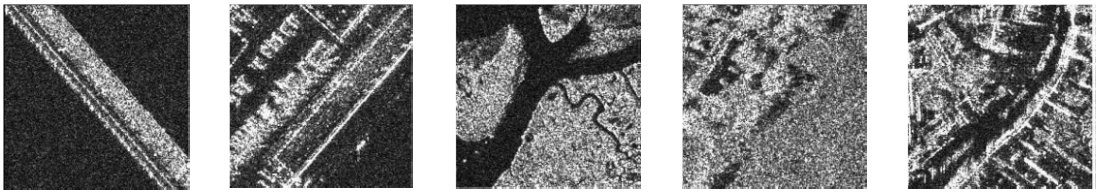

Bridge Harbour River deposit Veg. & forest Urban

Figure 2-4: Five example classes and the semantic labels are bridge, harbor, river deposit, vegetation and forest, urban.

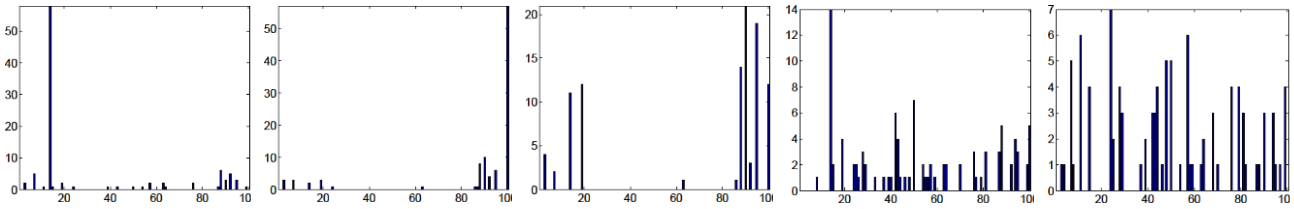

Bridge Harbour River deposit Veg. & forest Urban

Figure 2-5: From left to right, the word histograms of the 1st (bridge), 2nd (harbor), 3rd (river deposit), 4th (vegetation and forest), and 5th (urban) class after incorporating the mean ratios.

As an example, the histograms of the orientation and differential excitation for SAR images from 5 classes are shown in Figure 2-6. As can be seen, the adapted WLD is discriminative for structure. Visually, the 5 classes can be well discriminated.

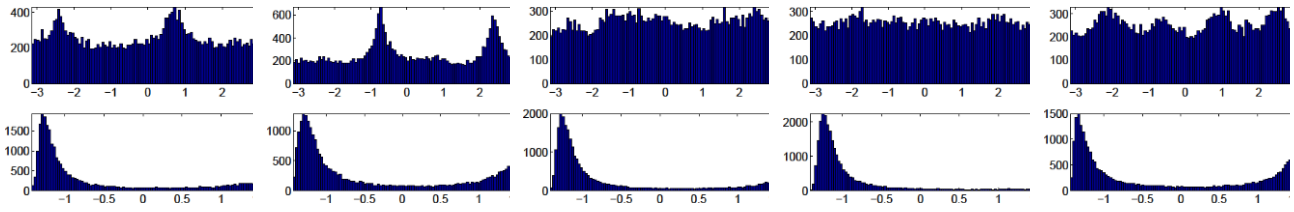

Bridge Harbour River deposit Veg. & forest Urban

Figure 2-6: From left to right, the histograms of orientation and differential excitation the 1st (bridge), 2nd (harbor), 3rd (river deposit), 4th (vegetation and forest), and 5th (urban) class after incorporating the mean ratios.

Based on the two adapted components $\theta(x_c)_{SAR}$ and $\xi(x_c)_{SAR}$, WLD for SAR images can be defined as the joint histogram $H\left(\xi(x_c)_{SAR}, \theta(x_c)_{SAR}\right)$. Therefore, there are two adjustable parameters, the number of bins for excitation C and orientation T. Following the same strategy as WLD, this joint histogram is converted to a one dimensional histogram. The adapted WLD includes not only local statistics but also local structure information, resulting in an improved performance in SAR image indexing.

2.3.1 *Adapted Weber local descriptor based feature descriptor*

The adaptation of WLD to SAR images by substituting the gradient with the ratio of mean differences in vertical and horizontal directions. For feature extraction using A-WLD, the involved parameters (the number of bins for orientation, C and excitation,T) are set $C = 18$ and $T = 8$. This will provide us a feature descriptor of size 144. Furthermore, the window size used in local feature extraction for the A-WLD is 7 pixels. The adapted WLD includes not only local statistics but also local structure information, resulting in an improved performance in SAR image indexing

3. Implementation

This chapter provides a brief overview of the implementation issues pertaining to the feature extraction algorithms and DMG in general. Feature extraction algorithms are invoked in the DMG module. During the running of DMG module, each product image is tiled into patches and the features are extracted and stored into the XML file. DMG requires operating parameters to start, but the parameters related to the feature extraction algorithms have been fixed after empirical evaluation of the selected values. Details of these parameters (operating and feature extraction algorithm related) are given in the Chapter 0.

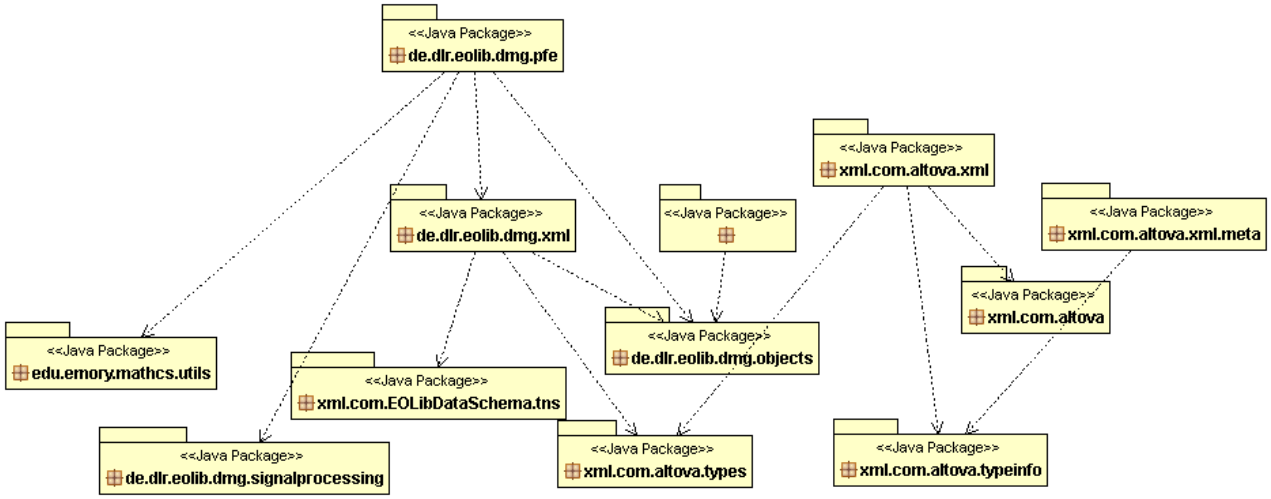

Figure 3-1: Class diagram of DMG constituting feature extraction algorithm implementation.

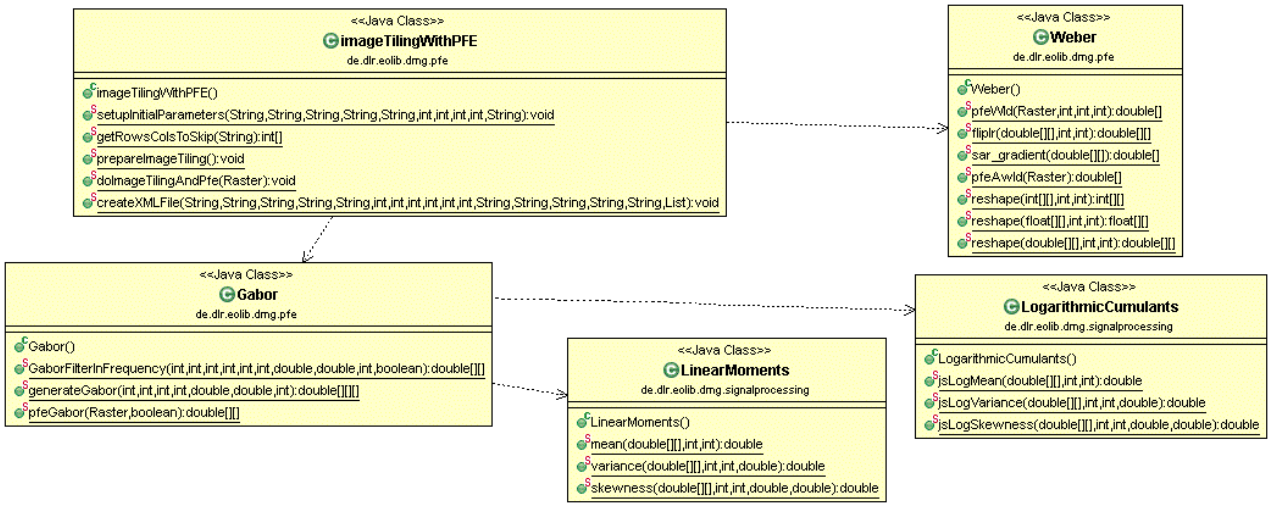

Figure 3-2: Class diagram of feature extraction algorithm implementation.

Extracted features are further utilized in the Image Information Mining (IIM) system [AD03] for fast indexing and annotation and Knowledge Discovery in Databases (KDD) exploration of large volume of Earth observation (EO) data archive, which works at patch level.

3.1 DMG implementation overview

Name		Data model generation		
Category	Feature extraction	**Uses**	DET SAR data	
Description	DMG constitutes of the following feature extraction algorithms: 1) Moments of the Gabor filtered images 2) Log-cumulants of the Gabor filtered images 3) Adapted WLD			
Data format	Features			
Programming language	Java	**Version**	21st July 2014	
Batch or Manual	Batch			
Operating system	Linux			
Compiler	Java 1.6 or later			

Pre-processing requirements	**Comments**	**Remarks**
Geometric correction	NA	
Radiometric correction	NA	
Other pre-processing	NA	

Parameters	**Comments**	**Remarks**
Input parameters	sourcePath - The absolute path of the L1B TerraSAR-X product. destinationPath - The absolute path of the EOLib destination directory where data model for this product need to be generated. operator - Name of the operator initiating the DMG. gridLevels - Indicator of which grid level is under consideration, valid argument in this version is '1'. multiTemporal - Flag if the ingestion catering multi temporal product or not, valid argument in this version is 'false'. tileSizeColumns - Width, i.e. number of columns of the image tile for DMG. tileSizeRows - Height, i.e. number of rows of the image tile for DMG. overlapColumns - Size of displacement of moving-window in image tile extraction in width or X-direction. overlapRows - Size of displacement of moving-window in image tile extraction in height or Y-direction.	Feature extraction specific fixed parameters: Gabor filter banks based features: Stages = 4. Orientations = 6. Lower frequency = 0.05. Upper frequency = 0.45. Adapted WLD based features: C - Number of excitation levels = 18. T - Number of orientations = 8. These values have been chosen empirically after several experiments on test data.
Output results	Quicklook - of TerraSAR-X image product in JPEG format. EOLib-xml file - containing metadata of product and image tiles. Quicklooks - of image tiles in JPEG format.	Files will be generated in the <destinationPath> directory.

3.2 Operating Hints

The software sub-system is operated on command line with nine arguments as follows:

$ java -jar dmg.jar <sourcePath> <destinationPath> <operator> <tileSizeColumns> <tileSizeRows> <gridLevels> <multiTemporal> <overlapColumns> <overlapRows>

The description of arguments is as follows:

Argument number	Argument name	Argument description
arg[0]	sourcePath	The absolute path of the L1B TerraSAR-X product.
arg[1]	destinationPath	The absolute path of the EOLib destination directory where data model for this product need to be generated.
arg[2]	operator	Name of the operator initiating the DMG.
arg[3]	tileSizeColumns	Width, i.e. number of columns of the image tile for DMG, suggested value in this version is ‘256’. Range of other suggested values is ‘256 to 512’. There is no default value set in this version.
arg[4]	tileSizeRows	Height, i.e. number of rows of the image tile for DMG, suggested value in this version is ‘256’. Range of other suggested values is ‘256 to 512’. There is no default value set in this version.
arg[5]	gridLevels	Indicator of which grid level is under consideration, valid argument in this version is '1'.
arg[6]	multiTemporal	Flag if the ingestion catering multi temporal product or not, valid argument in this version is 'false'.
arg[7]	overlapColumns	Size of displacement of moving-window in image tile extraction in width or X-direction, suggested value in this version is ‘128’. Range of other suggested values is ‘tileSizeColumns/2 to tileSizeColumns’. There is no default value set in this version.
arg[8]	overlapRows	Size of displacement of moving-window in image tile extraction in height or Y-direction, suggested value in this version is ‘128’. Range of other suggested values is ‘tileSizeRows/2 to tileSizeRows’. There is no default value set in this version.

3.3 Expected Output

A new folder with the same name as product directory containing following files will be generated in the <destinationPath> directory:

- Quicklook of TerraSAR-X image product in JPEG format.
- EOLib-xml file containing metadata of product and image tiles. Metadata also includes the extracted features, i.e. Moments and log-cumulants of the Gabor filtered images and adapted WLD features for each image tiles.
- Quicklooks of image tiles in JPEG format.

Appendix A Abbreviations

A-WLD	Adaptive Weber Local Descriptor
DET	Detected data
DMG	Data Model Generation
EO	Earth Observation
GEF	Gabor elementary functions
KDD	Knowledge Discovery in Databases
IIM	Image Information Mining
MoLC	Method of log-cumulants
RMD	Ratio of Mean Differences
SAR	Synthetic Aperture Radar
TN	Technical Note
WLD	Weber Local Descriptor

Appendix B References

Bovik, A., Clark, M. & Geisler, W., 1990. Multichannel Texture Analysis using Localized Spatial Filters. *Pattern Analysis and Machine Intelligence, IEEE Transactions on ,* 12(1), pp. 55-73.

Chen, J. et al., 2010. WLD: A Robust Local Image Descriptor. *Pattern Analysis and Machine Intelligence, IEEE Transactions on,* 32(9), pp. 1705-1720.

Cui, S., Dumitru, C. & Datcu, M., 2013. Ratio-Detector-Based Feature Extraction for Very High Resolution SAR Image Patch Indexing. *Geoscience and Remote Sensing Letters, IEEE,* 10(5), pp. 1175-1179.

Dunn, D., Higgins, W. & Wakeley, J., 1994. Texture Segmentation using 2-D Gabor Elementary Functions. *Pattern Analysis and Machine Intelligence, IEEE Transactions on,* 16(2), pp. 130-149.

Gabor, D., 1946. Theory of communication. Part 1: The analysis of information. *Electrical Engineers - Part III: Radio and Communication Engineering, Journal of the Institution of,* 93(26), pp. 429-441.

Julesz, B., 1981. Textons, the Elements of Texture Perception, and Their Interactions. *Nature,* 290(5802), pp. 91-97.

Kamarainen, J.-K., Kyrki, V. & Kälviäinen, H., 2006. Invariance properties of Gabor filter-based features-overview and applications. *Image Processing, IEEE Transactions on ,* 15(5), pp. 1088-1099.

Kandaswamy, U., Adjeroh, D. & Lee, M., 2005. Efficient Texture Analysis of SAR Imagery. *Geoscience and Remote Sensing, IEEE Transactions on,* 43(9), pp. 2075-2083.

Manjunath, B. & Ma, W., 1996. Texture Features for Browsing and Retrieval of Image Data. *Pattern Analysis and Machine Intelligence, IEEE Transactions on,* 18(8), pp. 837-842.

Mikolajczyk, K. & Schmid, C., 2005. A performance evaluation of local descriptors. *Pattern Analysis and Machine Intelligence, IEEE Transactions on,* 27(10), pp. 1615-1630.

Nicolas, J., 2002. Introduction to second kind statistics: application of Log-moments and Log-cumulants to SAR image law analysis. *Traitement du Signal,* 19(3), pp. 139-167.

Qian, S. & Chen, D., 1993. Discrete Gabor Transform. *Signal Processing, IEEE Transactions,* Volume 41, pp. 2429-2438.

Randen, T. & Husoy, J., 1999. Filtering for texture classification: a comparative study. *Pattern Analysis and Machine Intelligence, IEEE Transactions on,* 21(4), pp. 291-310.

Riaz, F., Silva, F., Ribeiro, M. & Coimbra, M., 2012. Invariant Gabor Texture Descriptors for Classification of Gastroenterology Images. *Biomedical Engineering, IEEE Transactions,* 59(10), pp. 2893-2904.

Sikora, T., 2001. The MPEG-7 visual standard for content description-an overview. *Circuits and Systems for Video Technology, IEEE Transactions on ,* 11(6), pp. 696-702.

Singh, J. & Datcu, M., 2013. SAR Image Categorization With Log Cumulants of the Fractional Fourier Transform Coefficients. *Geoscience and Remote Sensing, IEEE Transactions on ,* 51(12), pp. 5273-5282.

Super, B. & Bovik, A., 1991. Three-dimensional orientation from texture using gabor. *Visual Communications and Image Processing '91: Image Processing,* Volume 1606.

Touzi, R., Lopes, A. & Bousquet, P., 1988. A statistical and geometrical edge detector for SAR images. *Geoscience and Remote Sensing, IEEE Transactions on,* 26(6), pp. 764-773.